

# Relation Between Photoionisation Cross Sections and Attosecond Time Delays

Jia-Bao Ji<sup>1,\*</sup>, Anatoli S. Kheifets<sup>2,†</sup>, Meng Han<sup>3,‡</sup>,  
Kiyoshi Ueda<sup>1,4,5,¶</sup> and Hans Jakob Wörner<sup>1,§</sup>

<sup>1</sup> Laboratorium für Physikalische Chemie, ETH Zürich, 8093 Zürich, Switzerland

<sup>2</sup> Research School of Physics, The Australian National University, Canberra ACT 2601, Australia

<sup>3</sup> J. R. Macdonald Laboratory, Department of Physics, Kansas State University, Manhattan, KS 66506, USA

<sup>4</sup> Department of Chemistry, Tohoku University, Sendai, 980-8578, Japan

<sup>5</sup> School Physical Science and Technology, ShanghaiTech University, Shanghai 201210, China

E-mail: \* jiabao.ji@phys.chem.ethz.ch, † a.kheifets@anu.edu.au,

‡ mengh@phys.ksu.edu, ¶ kiyoshi.ueda@tohoku.ac.jp,

§ hwoerner@ethz.ch

**Abstract.** Determination and interpretation of Wigner-like photoionisation delays is one of the most active fields of attosecond science. Previous results have suggested that large photoionisation delays are associated with structured continua, but a quantitative relation between photoionisation cross sections and time delays has been missing. Here, we derive a Kramers-Kronig-like relation between these quantities and demonstrate its validity for (anti)resonances. This new concept defines a topological analysis, which rationalises the sign of photoionisation delays and thereby sheds new light on a long-standing controversy regarding the sign of the photoionisation delay near the Ar 3s Cooper minimum. Our work bridges traditional photoionisation spectroscopy with attosecond chronoscopy and offers new methods for analysing and interpreting photoionisation delays.

## 1. Introduction

Photoionisation is one of the fundamental processes that has been employed to reveal the electronic structure and dynamics of matter. Traditionally, photoionisation spectroscopy has been realised in the frequency domain by measuring the yield and angular distributions of photoelectrons [1, 2]. Newly developed laser-assisted interferometric techniques expanded these studies into the time domain and heralded the advent of attosecond science [3, 4]. The methods of attosecond streaking [5, 6] and reconstruction of attosecond beating by interference of two-photon transitions (RABBIT) [7, 8] were particularly instrumental in this new field. With these metrologies, photoionisation dynamics becomes directly accessible on the attosecond scale [9, 10], yielding the Wigner-like time delay [11–13], which describes the phase variation over the photoelectron energy. When reviewing the numerous measurements and calculations of photoionisation delays that have been reported to date, it becomes apparent that large photoionisation delays (in magnitude) are usually associated with structures in the photoionisation continuum, such as Fano resonances [14–16], shape resonances [17–22] and Cooper minima [23, 24]. For example, in the case of  $\text{CF}_4$ , photoionisation delays of up to  $\sim 600$  as have been measured and shown to originate from trapping of the outgoing photoelectron in a molecular shape resonance, whereby the trapping time is exacerbated by a molecular cage effect [19]. Naturally, this shape resonance also manifests itself as a local enhancement of the photoionisation cross section, but the width of the associated resonance cannot be trivially related to the trapping time, as discussed in [19]. In the simple case of a single continuum channel and single partial wave, the cross section of the shape resonance can be related directly with the corresponding time delay [25]. However, the interference between resonant and non-resonant photoionisation channels causes a more complex relationship between the time- and frequency-domain manifestations of photoionisation dynamics [26]. Do these results imply that no simple relationship between these two facets of photoionisation exists at all?

In this work, we derive a surprisingly simple and general relationship between the energy dependence of photoionisation cross sections and attosecond photoionisation delays. We demonstrate the validity of this relation for energetically confined (anti)resonances. In addition to linking in a quantitative manner time- and frequency-resolved photoionisation spectroscopies without restrictive assumptions, our results introduce a topological analysis, which explains why and under which circumstances the sign of photoionisation delays at (anti)resonances can change from one calculation to another. Such results have led to a notable controversy regarding the Cooper minimum (CM) in the  $3s$  continuum of argon, that is induced from the  $3p$  continuum through inter-shell correlation. Whereas some calculations have reported positive photoionisation delays near the  $3s$  CM [27–29], other calculations have reported negative delays [30, 31], whereas the authors of [30] later corrected their result and reported a positive delay [29]. Our present method shows that the local sign of these delays is related to the topology of the complex-valued photoionisation matrix element, i.e. its winding

number in the complex energy plane. This explains why, contrary to current belief, a quantitative reproduction of the cross section is not sufficient to guarantee the accuracy of calculated photoionisation delays. The topological analysis of the trajectories of the transition amplitudes is likely to facilitate the interpretation of photoionisation delays in structured continua and thereby to become a powerful and widely applicable approach for extracting the physics responsible for non-trivial photoionisation delays.

## 2. Results and discussions

### 2.1. Complex photoionisation time delay and the Wigner time delay

The angle-differential and angle-integrated photoionisation cross sections of single-photon ionisation (in the length gauge) can be expressed via the corresponding dipole transition amplitudes as [32, 33]

$$\sigma(E, \hat{\mathbf{k}}) = \frac{\pi}{3c} E |D(E, \hat{\mathbf{k}})|^2 = \frac{\sigma(E)}{4\pi} \left( 1 + \beta(E) P_2 \left( \cos(\hat{\mathbf{k}} \cdot \hat{\mathbf{e}}) \right) \right) \quad (1)$$

$$\sigma(E) = \frac{4\pi^2}{3c} E |D(E)|^2. \quad (2)$$

Here  $E$  denotes the photon energy,  $\hat{\mathbf{k}}$  and  $\hat{\mathbf{e}}$  are the unit vectors pointing to the emission and polarisation directions, respectively, and  $c$  is the speed of light  $\ddagger$ . The angular dependence in expression (1) enters via the angular anisotropy parameter  $\beta$  and the second Legendre polynomial  $P_2$ .

The Wigner time delay [11–13] is defined as

$$\tau(E) = \frac{\partial \arg\{D(E)\}}{\partial E} = \frac{\partial \text{Im}\{\ln(D(E))\}}{\partial E} = \text{Im} \left\{ \frac{\partial \ln(D(E))}{\partial E} \right\}. \quad (3)$$

Photoionisation can be regarded as a half-scattering process [34], and its transition amplitude can be presented by the  $S$ -matrix or the related  $R$ -matrix [35]. If the  $S$ -matrix is diagonalised with respect to the angular momentum  $\ell$  as

$$S(k) = \sum_{\ell, m} |\ell, m\rangle e^{2i\phi_\ell} \langle \ell, m| \quad (4)$$

with  $2\phi_\ell$  being the  $\ell$ -th scattering phase shift, then the photoionisation amplitude corresponds to

$$S(k) - 1 = \sum_{\ell, m} |\ell, m\rangle (e^{2i\phi_\ell} - 1) \langle \ell, m| = 2i \sum_{\ell, m} |\ell, m\rangle e^{i\phi_\ell} \sin \phi_\ell \langle \ell, m|. \quad (5)$$

Here the eigenvalues have no longer moduli of 1, and the phases are halved. Equation (3) yields  $\tau_\ell(E) = \partial \phi_\ell / \partial E$ , which is the original time delay proposed by Wigner [12]. The experimental time delay, on the other hand, is usually expressed in the  $\hat{\mathbf{k}}$ -space with interference of different  $\ell$ 's. Nonetheless, equation (3) can be interpreted as the “generalised Wigner delay”, which deals with the off-diagonal terms following Eisenbud's

$\ddagger$  In the atomic units which are in use here and throughout with  $e = m = \hbar = 1$  and  $c \approx 137$ . The atomic unit of time 1 a.u. = 24.2 as.

formula [11, 13, 36]. The analyticity of the  $S$ -matrix based on causality has been intensely studied [37–44] and the scattering amplitude was shown to be analytical in the upper-half complex  $k$ -plane for the physical region of the reaction, where  $k$  is the incident momentum. This is the foundation of the complex-scaling method for practical computations [45–47]. On the other hand, the analyticity can also be expressed regarding energy, and by applying the energy-time uncertainty principle, a time-domain picture of the scattering processes arises [48–50], where the connection of this “microscopic” time and the attosecond time delay is discussed in the next section. The analyticity leads to the Kramers-Kronig (KK) relations [51–53] that allow one to construct an energy-dependent complex function  $f(E)$  using only its real or imaginary part. Previous works have used the absorption cross section as the imaginary part to reconstruct the frequency-domain response function of materials, where the time-domain dynamics can be retrieved from their Fourier transform [54–56]. In this work we show that using the analyticity of the ionisation amplitude,  $\text{Im}\{\ln(D(E))\}$  is similarly connected to its real part, and the Wigner time delay can be retrieved via (3). The KK relation in the present form requires that the absorption variation vanishes beyond a certain frequency region, which is true for an (anti)resonance where the cross section below and above the resonance region (in the vicinity of the resonant energy  $E_r$ ) can be approximated as constant, and if the variation of  $E$  in equation (1) is negligible compared to the drastic modulation of  $D(E)$ ,  $\ln(\sigma(E)/\sigma_0)$  can be used instead of  $\ln((\sigma(E)/\sigma_0)/(E/E_0))$ , where  $\sigma_0$  and  $E_0$  are unitaries for the cross section and energy, respectively. The relation between the modulus of  $D(E)$  and the cross section  $\sigma(E)$  can be expressed as:

$$|D(E)| = \sqrt{\frac{3c}{4\pi^2 E} \sigma(E)} \quad (6a)$$

$$\ln(|D(E)|) = \text{Re}\{\ln(D(E))\} = \frac{1}{2} \ln\left(\frac{\sigma(E)/\sigma_0}{E/E_0}\right) + \text{const.} \approx \frac{1}{2} \ln\left(\frac{\sigma(E)}{\sigma_0}\right) + \text{const.} \quad (6b)$$

The trajectory of  $D(E)$  from  $E \ll E_r$  to  $E \gg E_r$  is approximately a closed contour on the complex plane, as shown in figure 1 (e) and (j). Using the KK relations of the amplitude and the phase of a complex function, it has been shown [57–63] that the phase can be retrieved (with a freedom of a common phase shift) from the absolute value when  $\ln(D(E))$  vanishes faster than  $E^{-1}$  and  $D(E)$  fulfils the minimum-phase condition, namely, that all the poles and zeros are located in the same half-plane. This means that the origin is not enclosed in the trajectory of  $D(E)$  (the winding number is 0), and the total phase change throughout the (anti)resonant region is 0 instead of  $\pm 2\pi$  [61, 63].

In the interaction picture  $\hat{H}(\Delta t) = \hat{H}_0 + \hat{H}_1(\Delta t)$ , where  $\hat{H}_0$  is the field-free Hamiltonian, and  $\hat{H}_1(\Delta t)$  is the interaction term as a function of retardation, the interaction is turned on at  $\Delta t = 0$ , which triggers a transition at  $\Delta t \geq 0$ . This retardation is the “microscopic” time introduced by Branson [48], and we have ignored the relativistic effect of the virtual-particle “cloud”, whose temporal feature is much shorter than the electronic response in atoms (molecules), as analogously shown in a

previous study [50]. Thus, in the energy (frequency) domain, we have

$$D(E) = \int_{-\infty}^{+\infty} \tilde{D}(\Delta t) e^{iE\Delta t} d\Delta t = \int_0^{+\infty} \tilde{D}(\Delta t) e^{iE\Delta t} d\Delta t \quad (7)$$

where  $\tilde{D}(\Delta t)$  has the form:

$$\tilde{D}(\Delta t) = \begin{cases} \frac{1}{2\pi} \int_{-\infty}^{+\infty} D(E) e^{-iE\Delta t} dE & \text{for } \Delta t \geq 0 \\ 0 & \text{for } \Delta t < 0 \end{cases}. \quad (8)$$

The case of  $\Delta t \geq 0$  corresponds to the time propagation of a superposition state, while the elimination of the transition amplitude for  $\Delta t < 0$  reflects the causal condition. If we perform analytical continuation of  $E = \mathcal{E} + i\mathfrak{E}$ , where  $\mathcal{E}$  and  $\mathfrak{E}$  are real and  $\mathfrak{E} > 0$ , equation (7) becomes:

$$D(E) = D(\mathcal{E} + i\mathfrak{E}) = \int_0^{+\infty} \tilde{D}(\Delta t) e^{i\mathcal{E}\Delta t} e^{-\mathfrak{E}\Delta t} d\Delta t. \quad (9)$$

Since the dipole transition amplitude of real energy  $D(\mathcal{E}) = \int_0^{+\infty} \tilde{D}(\Delta t) e^{i\mathcal{E}\Delta t} d\Delta t$  converges and  $e^{-\mathfrak{E}\Delta t}$  is a bounded and monotonically decreasing real function for  $\Delta t \geq 0$ , equation (9) fulfils the Abel-Dirichlet test of convergence for improper integrals and thus converges [64, 65]. This ensures that  $D(E)$  has no poles in the upper-half of the complex energy plane §.

From expression (7), we can define the complex “average retardation”, with the same expression derived by Pollak and Miller [66, 67], as

$$\mathfrak{T}(E) = \frac{\int_0^{+\infty} \Delta t \tilde{D}(\Delta t) e^{iE\Delta t} d\Delta t}{\int_0^{+\infty} \tilde{D}(\Delta t) e^{iE\Delta t} d\Delta t} = \frac{1}{i} \frac{1}{D(E)} \frac{\partial D(E)}{\partial E} = \frac{1}{i} \frac{\partial \ln(D(E))}{\partial E}. \quad (10)$$

If we assume that the minimum-phase condition is fulfilled (we shall come back to this point in the discussion of the CM), the Wigner time delay  $\tau(E)$  is connected to  $\mathfrak{T}(E)$  and  $\sigma(E)$  using equations (3) and (6b) and the KK relations by applying the logarithm Hilbert transform (LHT):

$$\begin{aligned} \tau(E) &= \text{Im}\{i\mathfrak{T}(E)\} = \text{Re}\{\mathfrak{T}(E)\} = -\mathcal{H}\{\text{Im}\{\mathfrak{T}(E)\}\} \\ &= \frac{1}{2} \frac{\partial}{\partial E} \mathcal{H}\{\ln(\sigma(E))\} = \frac{1}{2} \mathcal{H}\left\{ \frac{1}{\sigma(E)} \frac{\partial \sigma}{\partial E} \right\} \end{aligned} \quad (11)$$

where  $\mathcal{H}$  is the Hilbert transform:

$$\mathcal{H}\{f(E)\} = \frac{1}{\pi E} \otimes f(E) = \frac{1}{\pi} \mathcal{P} \int_{-\infty}^{+\infty} \frac{f(E')}{E - E'} dE' \quad (12)$$

which is linear and commutative to the derivative. Here  $\otimes$  represents the convolution, and  $\mathcal{P}$  refers to the Cauchy principal value.

Relation (11) establishes the general method to retrieve the Wigner time delay from the photoionisation cross section. However, as the integral (12) runs from  $-\infty$  to

§ Unlike  $D(E)$ , any pole of  $\sigma(E) \propto |D(E)|^2$  will have a complex conjugate pole on the other half plane, since  $|D(E)|^2 = D(E)D^*(E)$ . Both  $D(E)$  and  $D^*(E)$  correspond to the same  $\sigma(E)$ , but  $D^*(E)$  has the opposite phase, which corresponds to the reversed causality.

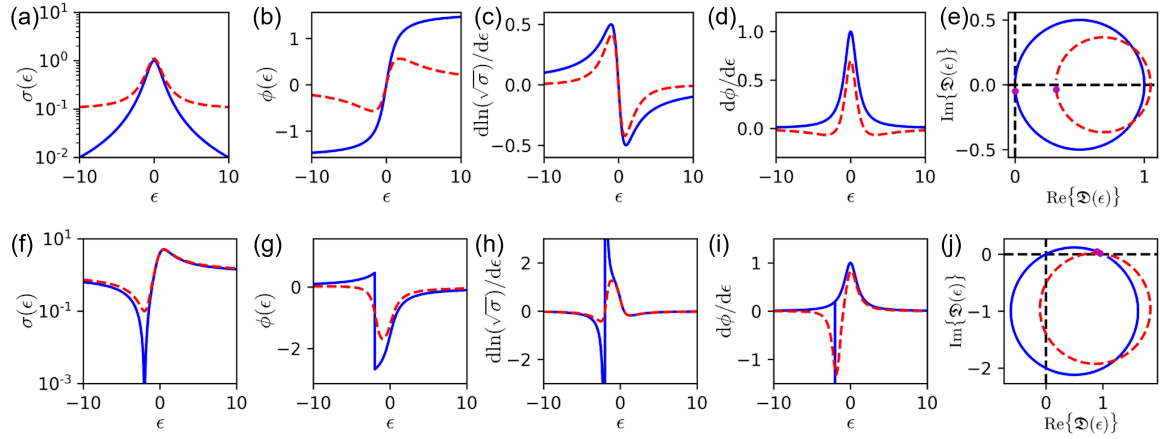


**Figure 1. Transition amplitudes for the Lorentz and Fano resonances.** Cross sections (**a**, **f**), phases (**b**, **g**), the derivatives of the logarithm of the cross sections (**c**, **h**), Wigner time delays (**d**, **i**), and transition-amplitude trajectories (**e**, **j**) for the Lorentzian lineshape (**a-e**) and the Fano lineshape with  $q = 2$  (**f-j**), respectively, where the blue solid lines correspond to  $\sigma_a = 1$  and  $\sigma_b \rightarrow 0^+$ , while the red dashed lines correspond to  $\sigma_a = 1$  and  $\sigma_b = 0.1$ . The magenta dots in (**e**) and (**j**) indicate the beginning of the trajectories at  $\epsilon \rightarrow -\infty$ .

$+\infty$ , including the bound states for the negative part, using the whole profile of the photoionisation cross section is not practical. Instead, one can investigate the behaviour near a resonance with energy  $E_r$  above the threshold, for instance, the shape resonance, where the variation of the transition amplitude rapidly decays beyond a relatively small energetic window in the vicinity of  $E_r$ , and the Wigner time delay shows thus local behaviour within this region. The boundary conditions at (positive and negative) infinity hence become

$$\lim_{(E-E_r) \rightarrow \infty} \frac{|E - E_r|}{\sigma(E)} \frac{\partial \sigma}{\partial E} = 0. \quad (13)$$

For example, for the Lorentzian profile, the cross-section variation  $\partial \sigma / \partial E$  is proportional to  $|E - E_r|^{-3}$ . If we assume that  $\sigma(E)$  outside the resonant region is approximately constant due to the contribution of the non-resonant channels, expression (13) is fulfilled. In the following sections, we will give the analytical expressions of the Wigner time delay for the Lorentzian and Fano lineshapes using LHT. We will demonstrate that LHT is also applicable to resonances with multi-peak features, for example, the xenon giant resonance modulated by a  $C_{60}$  cage. Finally, we will examine the Cooper minima and discuss the role of the minimum-phase condition, i.e. the winding number of the trajectory.

## 2.2. (Anti)resonances with Lorentzian and Fano lineshapes

The cross section of an (anti)resonance can be expressed by the Lorentzian lineshape, e.g., the Breit-Wigner resonance formula [68, 69]:

$$\sigma_L(\epsilon) = \sigma_a \frac{1}{\epsilon^2 + 1} + \sigma_b \quad (14)$$

or the Fano lineshape [70, 71]:

$$\sigma_F(\epsilon) = \sigma_a \frac{(\epsilon + q)^2}{\epsilon^2 + 1} + \sigma_b \quad (15)$$

where  $\epsilon = (E - E_r)/(\Gamma/2)$  is the relative energy, and  $\sigma_a$  and  $\sigma_b$  are the resonant and non-resonant cross sections, respectively. We assume that the corresponding pathways contribute to the overall transition amplitude coherently, which fits in the Feshbach picture [72] and was recently demonstrated in the X-ray regime [73]. The Lorentzian lineshape is symmetric, while the Fano lineshape is asymmetric, with  $q$  being the asymmetric parameter.  $\Gamma$  describes the peak width and thus the resonant state has a lifetime of  $1/\Gamma$  from Fano's picture. The cross section for a Lorentzian or Fano lineshape can be written as a common expression:

$$\sigma_{L/F}(\epsilon) = \mathfrak{S} \frac{(\epsilon + Q)^2 + \gamma^2}{\epsilon^2 + 1} . \quad (16)$$

For the Lorentzian lineshape,  $Q = 0$ ,  $\gamma^2 = 1 + \sigma_a/\sigma_b$ , where  $\mathfrak{S} = \sigma_b$ , while for the Fano lineshape,  $Q = q/(r+1)$ ,  $\gamma^2 = r(r+q^2+1)/(r+1)^2$ , where  $r = \sigma_b/\sigma_a$ , and  $\mathfrak{S} = \sigma_a + \sigma_b$ . The detailed proof can be found in Appendix A. Using  $\partial/\partial E = (2/\Gamma)\partial/\partial\epsilon$ , we have

$$\frac{1}{\sigma(E)} \frac{\partial \sigma}{\partial E} = \frac{2}{\Gamma} \left[ \frac{\frac{2}{\gamma} \left( \frac{\epsilon+Q}{\gamma} \right)}{\left( \frac{\epsilon+Q}{\gamma} \right)^2 + 1} - \frac{2\epsilon}{\epsilon^2 + 1} \right] . \quad (17)$$

It is easy to verify that the boundary conditions (13) are fulfilled, and (11) yields

$$\tau_{L/F}(E) = \frac{2}{\Gamma} \left[ -\frac{\frac{1}{|\gamma|}}{\left( \frac{\epsilon+Q}{|\gamma|} \right)^2 + 1} + \frac{1}{\epsilon^2 + 1} \right] . \quad (18)$$

Here we used the property of the Hilbert transform that  $\mathcal{H}\{f(aE)\}(E) = \text{sgn}(a) \times \mathcal{H}\{f(E)\}(aE)$ . The time delay can be decomposed as two Lorentzian peaks with widths of  $\gamma\Gamma$  and  $\Gamma$  and opposite signs, centred at  $(E_r - \frac{Q\Gamma}{2})$  and  $E_r$ , respectively. For the Fano lineshape, the positive and negative peaks are separated by  $Q\Gamma/2$ . When  $r \rightarrow 0$  and thus  $|\gamma| \rightarrow 0$ , the first time-delay peak approaches  $-\pi\delta(\epsilon + Q)$ . These correspond to the cases plotted in figure 1 (i). On the other hand, for the Lorentzian lineshape, since  $Q = 0$ , the two peaks are co-centred and their sum is symmetric. If  $\sigma_b/\sigma_a \rightarrow 0$  and thus  $|\gamma| \rightarrow \infty$ , the first peak vanishes and thus the time delay is a single Lorentzian peak with  $\tau(E_r) = 2/\Gamma$  at its centre, as discussed in [74]. For the general case, it corresponds to a narrower peak subtracted by a wider peak, yielding the alternating sign of the time delay. These cases are illustrated in figure 1 (d).

Since  $(Q + i\gamma)$  can be regarded as the “complex asymmetry parameter” [73], a more insightful approach is to investigate an analytical function that satisfies  $|\mathfrak{D}(\epsilon)|^2 = \sigma(\epsilon)$ , as proposed in [14, 75]:

$$\mathfrak{D}(\epsilon) = \sqrt{\mathfrak{S}} \frac{\epsilon + Q + i\gamma}{\epsilon + i} = \sqrt{\mathfrak{S}} \left[ 1 + \frac{Q + i(\gamma - 1)}{\epsilon + i} \right]. \quad (19)$$

It fulfils the minimum-phase condition when  $\gamma > 0$ , so  $\mathfrak{D}(\epsilon)$  is related to  $D(\epsilon)$  by multiplying  $\sqrt{\frac{4\pi^2 E}{3c}}$  and a common phase offset, namely  $D(\epsilon) = \sqrt{\frac{4\pi^2 E}{3c}} \mathfrak{D}(\epsilon) e^{i\phi_0}$ , where  $\sqrt{\frac{4\pi^2 E}{3c}}$  is approximately constant in the vicinity of the (anti)resonance, and

$$\begin{aligned} \arg \{D(\epsilon)\} &= \arg \{\mathfrak{D}(\epsilon)\} + \phi_0 = \arg \{\epsilon + Q + i\gamma\} - \arg \{\epsilon + i\} + \phi_0 \\ &= \cot^{-1} \left( \frac{\epsilon + Q}{\gamma} \right) - \cot^{-1}(\epsilon) + \phi_0. \end{aligned} \quad (20)$$

Therefore,  $D(\epsilon)$  and  $\mathfrak{D}(\epsilon)$  share the same Wigner time delay  $\tau(\epsilon) = \frac{2}{\Gamma} \partial \arg \{D(\epsilon)\} / \partial \epsilon$ , which is expressed by (18). The trajectory of  $\mathfrak{D}(\epsilon)$  from  $\epsilon \rightarrow -\infty$  to  $\epsilon \rightarrow +\infty$  is a counter-clockwise rotating (due to the causality) closed circle [14, 44] with the radius of  $\frac{\sqrt{\mathfrak{S}}}{2} \sqrt{(\gamma - 1)^2 + Q^2}$  centred at  $(\sqrt{\mathfrak{S}} \frac{\gamma+1}{2}, -\sqrt{\mathfrak{S}} \frac{Q}{2})$ . It can be easily verified that the origin is not enclosed when  $\gamma > 0$ . Take the Fano resonance as an example, at  $\epsilon \rightarrow \pm\infty$ , the transition amplitudes are dominated by the direct ionisation channel, which is approximately constant in this region. As  $r \rightarrow 0$  (“pure” Fano lineshape), the trajectory approaches tangential to the origin, where a  $(-\pi)$ -phase jump occurs within an infinitely small energy interval, which corresponds to the  $-\pi\delta(\epsilon + Q)$  peak. As  $\gamma$  deviates from 0, the maximal phase jump is  $2\text{sgn}(\gamma - 1)\cos^{-1} \left( 2\sqrt{\gamma}/\sqrt{(\gamma + 1)^2 + Q^2} \right)$  for  $\gamma \neq 1$  and  $\pm 2\tan^{-1}(Q/2)$  for  $\gamma = 1$  (see Appendix B for details). For the “pure” Lorentzian transition amplitude  $D(\epsilon) \propto (\epsilon + i)^{-1}$  [44], there is a phase offset of  $\pi$  between  $\epsilon \rightarrow +\infty$  and  $\epsilon \rightarrow -\infty$ , which does not fulfil the minimum-phase condition since it encloses “half” the origin. Its phase retrieved by the LHT method starts and ends at the same value at infinities, which corresponds to shifting the circle by an infinitely small amount away from the origin, and thus subtracts an infinitely broad Lorentzian lineshape according to (18), where  $Q = 0$  and  $\gamma \rightarrow +\infty$ . Its behavior near  $\epsilon = 0$ , which is of most interest, is largely unchanged. The maximal phase jump is  $4\tan^{-1}(\sqrt{\gamma}) - \pi = 4\tan^{-1}(\sqrt[4]{1 + \sigma_a/\sigma_b}) - \pi$ , which approaches  $\pi$  when  $\sigma_a/\sigma_b \rightarrow 0$ . Examples of Lorentzian and Fano lineshapes are plotted in figure 1, where the increase of  $\sigma_b/\sigma_a$  results in the decrease of the extreme(s) of the time delay.

In preceding work [25] the shape-resonance analysis was performed by utilising the relation  $\sigma_l(E) \propto \sin^2 \phi_l$  from equation (5), which is applicable if only one partial wave of angular momentum  $l$  is dominating. Assume that no background is contributing, and let  $f_l(E) = -\cot(\phi_l(E))$  be a real function, then

$$\sin^2(\phi_l(E)) = \frac{1}{f_l(E)^2 + 1} = \left| \frac{1}{f_l(E) \pm i} \right|^2. \quad (21)$$



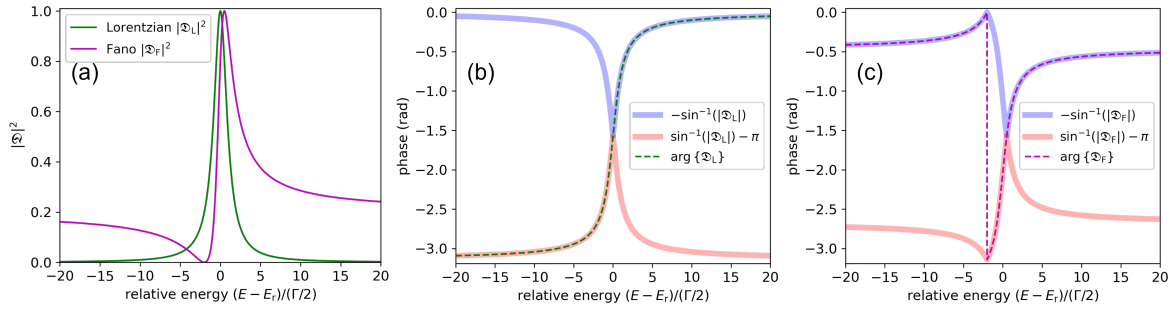


**Figure 2. Phase retrieval for Lorentzian and Fano lineshapes using  $\sigma_l(E) \propto \sin^2 \phi_l$ .** Normalized cross section of the Lorentzian and Fano lineshapes with  $\sigma_b = 0$  are plotted in (a). For the Lorentzian lineshape  $\mathfrak{D}_L(\epsilon) = 1/(\epsilon + i)$ , while for the Fano lineshape  $\mathfrak{D}_F(\epsilon) = (\epsilon + q)/((q + i)(\epsilon + i))$ , where  $q = 2$  is used for plotting. The phase of  $\mathfrak{D}(\epsilon)$  and the phase retrieved according to  $(\phi(\epsilon) = \sin^{-1}(|\mathfrak{D}(\epsilon)|))$  for the Lorentzian and Fano lineshapes are shown in (b) and (c), respectively. Note that adding the phase by a constant factor will not change the corresponding Wigner time delay defined in equation (3).

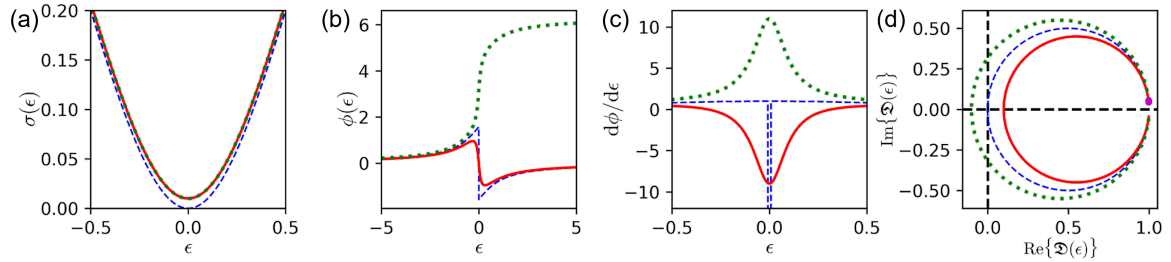


**Figure 3. Comparison of the trajectories with different topologies.** Cross sections in the vicinity of the minimum (a), phases (b), time delays (c), and trajectories (d, the magenta dot indicates  $\epsilon \rightarrow -\infty$ ) of the anti-Lorentzian lineshapes with  $\mathfrak{S} = 1$ ,  $Q = 0$  and  $\gamma = 0^+$  (blue, dashed), 0.1 (red, solid), or  $-0.1$  (green, dotted), according to (19).

Therefore, assuming  $f_l(E)$  to be analytical,

$$\mathcal{H}\left\{\frac{1}{2} \ln(\sigma_l(E))\right\} = -\arg\{f_l(E) \pm i\} = \mp \cot^{-1}(f_l(E)) = \pm \phi_l(E) \quad (22)$$

if one of the two branches  $(f_l(E) \pm i)$  has no poles or zeros on the upper half-plane of  $E$ . For example, let  $f_l(E) = \epsilon$ , where  $\epsilon = (E - E_{r,l})/(\frac{\Gamma_l}{2})$  and  $\Gamma_l > 0$ ,  $(f_l(E) + i)$  fulfils the condition and leads to the “pure” Breit-Wigner resonance with Lorentzian lineshape. For the “pure” Fano lineshape we have  $f_l(E) = (q\epsilon - 1)/(\epsilon + q)$  thus  $f_l(E) + i = (q + i)(\epsilon + i)/(\epsilon + q)$  also fulfils the requirement. Since  $\pm \phi_l(E)$  and  $\pi \pm \phi_l(E)$  yield the same value in expression (21), the Wigner time delay corresponds to  $\pm \partial \arg\{\phi_l(E)\}/\partial E$ , and the sign depends on different regions, as shown in figure 2.

In real experiments, the measurable energy range is finite and thus the boundary conditions are not strictly fulfilled. This leads to a deviation of the retrieved time delay from its physical counterpart. However, when comparing two photoionisation processes,

the relative time delay, which is usually the experimental observable [10], can be obtained from their cross-section ratio, which converges faster than the individual time delays:

$$\begin{aligned}\Delta\tau(E) &= \tau_1(E) - \tau_2(E) = \frac{\partial}{\partial E} \arg \left\{ \frac{D_1}{D_2} \right\} \\ &= \frac{1}{2} \frac{\partial}{\partial E} \mathcal{H} \left\{ \ln \left( \frac{\sigma_1}{\sigma_2} \right) \right\} = \frac{1}{2} \mathcal{H} \left\{ \frac{\sigma_2}{\sigma_1} \frac{\partial(\sigma_1/\sigma_2)}{\partial E} \right\} .\end{aligned}\quad (23)$$

This is particularly useful for comparing the same resonance under different surroundings, for example the giant resonance of xenon with and without a  $C_{60}$  cage, as discussed in the next section.

### 2.3. Composite resonances with more complicated features

We note that the amplitude-phase relation can be extended beyond “simple” resonances with Lorentzian or Fano lineshapes, as the derivation from the causality is more general than the specific models of transition amplitude. For example, the cross sections and time delays of free xenon and xenon in a  $C_{60}$  cage in the region of the giant resonance have been computed using the random-phase approximation (RPA), relativistic RPA (RRPA) [76], RPA with exchange (RPAE), and time-dependent Schrödinger equation (TDSE) methods [77]. As shown in figure 4, the cross-section ratio shows multiple peaks in the giant-resonance region, which reflects the influence of the  $C_{60}$  shell, and the time delay retrieved by the LHT, which does not require the phase of the transition amplitude, almost quantitatively agrees with the reported value obtained from the phase. Positive (negative) time delays are typically associated with local maxima (minima) of the cross-section ratio. The reconstructed trajectory of  $\mathfrak{D}_{\text{Xe}@C_{60}}/\mathfrak{D}_{\text{Xe}(\text{free})}$  has a multiple-spiral structure, which manifests the validity of the LHT method for complex resonances. This relies on the fact that the modulation of the  $C_{60}$  surroundings is smaller than the modulus of the transition amplitude *per se*, so that the transition-amplitude ratio lies around (1, 0) on the complex plane, as illustrated in figure 4 (b), which avoids encircling the origin, and its winding number can thus be taken to be zero.

### 2.4. Time delays near Cooper minima

The Cooper minima are antiresonances that have a distinctly different origin compared to the Fano or shape resonances [23, 78, 79]. Nevertheless, the cross section near the minimum can be locally fitted by a Fano lineshape with  $\gamma \rightarrow 0$  in expression (16) (see Appendix D for details). Although  $\pm\gamma$  give the same cross section, they have different topological structures on the complex plane. Only the transition amplitude corresponding to the positive  $\gamma$  is minimum-phase, which leads to a negative time delay and is expressed by (18) using the same fitting parameters, while the negative  $\gamma$  gives a positive time delay, as demonstrated in figure 3. We can quantify the relative shift of the trajectory by defining the parameter:

$$g = \frac{|\gamma|}{Q^2 + 1} \approx \sqrt{\frac{r}{q^2 + 1}} \quad (24)$$

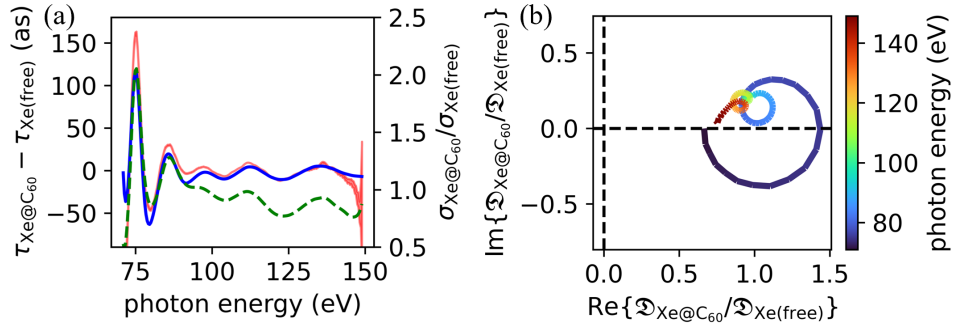


**Figure 4.** Applications of the LHT formalism to Xe and Xe@C<sub>60</sub>. (a) The calculated cross-section ratio (green dashed, right vertical axis) using the RPAE method and the time delay (blue, left vertical axis) [77] and the time delay retrieved from the cross sections using the LHT (red, left vertical axis). The filled area indicates the difference between first taking the energy derivative then perform the Hilbert transform and first performing the Hilbert transform then taking the energy derivative, which are the same when the boundary conditions are strictly fulfilled. (b) The transition-amplitude trajectory constructed by  $\mathfrak{D}_{\text{Xe@C}_{60}}/\mathfrak{D}_{\text{Xe(free)}} = \exp[\frac{1}{2}\ln(\mathfrak{r}) + \frac{i}{2}\mathcal{H}\{\ln(\mathfrak{r})\}]$ , where  $\mathfrak{r} = \sigma_{\text{Xe@C}_{60}}/\sigma_{\text{Xe(free)}}$  is the cross-section ratio.

which is the distance between the origins of the circles corresponding to  $\pm\gamma$ , divided by the average diameter, when  $r \approx 0$  and thus  $|\gamma| \ll 1$ . For example, in figure 3 (d),  $g = 0.1$ , where  $r \approx 0.01$  and  $q = 0$ .

For numerical illustration of the proposed technique, we analyse the time delay near the CM in various shells of noble gas atoms: Xe 4*d*, Ar 3*p* and Ar 3*s*. The Xe 4*d* and Ar 3*p* CM have a kinematic origin where the radial node in the target orbital passes through the oscillation in the continuum radial orbital. The case of Ar 3*s* is different as the corresponding CM is induced by the inter-shell correlation with the 3*p* shell. These two different cases of kinematic and correlation induced CM allows us to demonstrate the utility of the proposed technique. Our numerical illustrations are based on the RPAE calculations reported in [28], and more information can be found in Appendix C. First we evaluate the angle differential photoionisation cross section (1) in the zero emission direction  $\hat{\mathbf{k}} \parallel \hat{\mathbf{e}}$ . This cross section in the vicinity of the CM is fitted with the standard set of Fano parameters  $E_r$ ,  $\Gamma$ ,  $q$  and  $\rho^2$  [70, 71, 80]. Next, these parameters are converted to an alternative set  $Q$  and  $\gamma$  which allows to express the photoionisation amplitude  $\mathfrak{D}(E)$  (19, 20) and the corresponding time delay  $\tau(E)$  (18). These two quantities are compared with their numerical counterparts evaluated using the RPAE method.

This comparison is displayed in figure 5. Panels (a-c) show the photoionisation cross sections near the corresponding CM. In panels (d-f), the parametric plots exhibit the complex photoionisation amplitudes  $\mathfrak{D}(E)$  as given analytically by (19) and evaluated in the RPAE, respectively. The arrows in the amplitude graphs indicate the winding direction as the photon energy increases. In (g-i), we display the corresponding time delays. The three columns, from left to right, correspond to the Xe 4*d*, Ar 3*p* and Ar

3s orbitals, respectively. The LHT-extracted time delays given by (15) show very good agreement with the numeric results for Xe 4*d* and Ar 3*p*, while for the Ar 3*s* CM there is a qualitative disagreement that LHT yields negative delay at the cross-section minimum, while the computation suggests the opposite. Such a profound difference in time delays near the CM can be traced to the corresponding photoionisation amplitudes and their winding numbers, as plotted in panels (d-f). In the cases of Xe 4*d* and Ar 3*p*, both the analytical and numeric amplitudes do not encircle the origin and their respective winding numbers are 0. The case of Ar 3*s* is different where the RPAE amplitude encircles the origin, namely, the minimum-phase condition is not fulfilled. In equation (19), when  $\gamma < 0$ , the transition amplitude, denoted as  $\check{D}(\epsilon)$ , has a zero at  $(-Q + i|\gamma|)$  and thus has winding number of 1. The LHT-retrieved transition amplitude can be expressed as

$$\mathfrak{D}(\epsilon) = \frac{\epsilon + Q + i|\gamma|}{\epsilon + Q - i|\gamma|} \sqrt{\frac{3c}{4\pi^2 E}} \check{D}(\epsilon) e^{-i\phi_0} \quad (25)$$

which gives rise to a Lorentzian lineshape that should be added to the LHT-retrieved time delay:

$$\frac{\partial \arg\{\check{D}(\epsilon)\}}{\partial \epsilon} = \frac{\partial \arg\{\mathfrak{D}(\epsilon)\}}{\partial \epsilon} + \frac{\frac{2}{|\gamma|}}{\left(\frac{\epsilon+Q}{|\gamma|}\right)^2 + 1}. \quad (26)$$

Hence, (18) becomes

$$\check{\tau}(E) = \frac{2}{\Gamma} \left[ \frac{\frac{1}{|\gamma|}}{\left(\frac{\epsilon+Q}{|\gamma|}\right)^2 + 1} + \frac{1}{\epsilon^2 + 1} \right] \quad (27)$$

which turns the negative peak into a positive peak, and in the limit of  $\gamma \rightarrow 0^-$ , it becomes the  $+\pi\delta(\epsilon+Q)$  peak. The time delays near the CM for the zero-winding-number and one-winding-number trajectories are given by (18) and (27), respectively. Using equations (25, 27), the complex transition amplitude and the corresponding time delay of the Ar 3*s* CM with winding number equalling to 1 can be retrieved, as shown in panels (f) and (i) in figure 5, respectively. This gives a positive time delay that excellently agrees with the RPAE result, which indicates that the KK relations reduces the detailed time-delay computation into the quantitative winding-number determination, as long as the cross section is available experimentally or theoretically.

The validity of the relation between cross section and time delay for the CM of Ar 3*p* can be examined by the RABBIT experiment measuring the group delay of photorecombination upon high harmonic generation (HHG) [23], which can be physically understood as the inverse process of the photoionisation. As discussed in [29], the transition amplitudes of the two processes are equal and therefore feature the same time delay. The concurrence of the photoionisation cross section and photorecombination probability has been demonstrated by HHG studies [79,81]. Figure 5(h) manifests the agreement of time delay between the experimental results and the RPAE calculation [82] and the analytical model with Fano parameters. The experiment therefore verifies that

the winding number of the transition amplitude for Ar  $3p$  CM is 0, and as long as the winding number is determined, the time delay can be derived from the cross section variation at the CM. On the other hand, theoretical calculations yield winding number of 1 for the Ar  $3s$  CM, as the trajectory of the transition amplitude encircles the origin, as shown in figure 5(f). However, the RABBIT measurement reported in [24] suggests that the time delay of Ar  $3s$  CM is more negative than that of Ar  $3p$ , which contradicts the theoretical calculations. As compared in figure 6, with the fitted Fano parameters from the computed cross sections, assuming that Ar  $3s$  has winding number of 1 at CM, the retrieved relative time delay between Ar  $3s$  and  $3p$  matches the computation, while assuming that Ar  $3s$  has winding number of 0 at CM leads to a better agreement with the measured values which strikingly deviate from the theoretical prediction with the opposite sign. This indicates that the other pathways, e.g. the shake-up channels, shift the trajectory near the origin, so that the winding number changes from 1 to 0 and leads to a negative delay. We note that for the Xe  $4d$  or the Ar  $3p$  CM, the kinematic node appears only in one of the two photoionisation channels, which is offset by a finite contribution from the another channel, while for the Ar  $3s$  CM, the  $3s \rightarrow Ep$  channel is the only channel, if the target-state channel coupling is neglected. In this case, the trajectory exactly crosses the origin on the complex plane and leads to the discontinuity of the phase and thus a  $\delta$ -function time delay with arbitrary sign. Therefore, the finite time delay only comes from those couplings, and its sign depends on the detailed coupling terms. In fact, the subtle shift of the trajectory with  $g = 0.046$  causes the topological change and thus flips the time delay and leads to a deviation of more than 1000 as.

### 3. Conclusions

In conclusion, we have introduced a Kramers-Kronig-like relation between photoionisation cross sections and attosecond time delays, which relies on the general properties of coherence and causality of the transition amplitude. We have derived a unified time-delay formula of Lorentzian and Fano lineshapes with constant and coherent background, where both Breit-Wigner and Fano resonances correspond to a pair of Lorentzian time-delay peaks with opposite signs. We analysed several cases of the CM in valence shells of noble gas atoms. The relation is manifested by the excellent agreement of the retrieved time delays near CM of Xe  $4d$  and Ar  $3p$  from their cross sections, in comparison to the calculated time delay by RPAE. The LHT further requires the topological property that the trajectory has winding number of 0, which is particularly relevant for antiresonances where the minimal cross section approaches zero. The theoretical calculations suggest that Xe  $4d$  and Ar  $3p$  have winding number of 0 at CM, whereas Ar  $3s$  has winding number of 1 at CM. The photorecombination experiment at Ar  $3p$  CM [23] shows good agreement with the computation and the analytical Fano model with winding number of 0. The latest experimental results on photoionisation [24] rather hint at a negative time delay near the CM of Ar  $3s$ , which is at variance with the RPAE [28] and TDLDA [29] predictions and suggests a winding number of 0. So this particular case remains con-

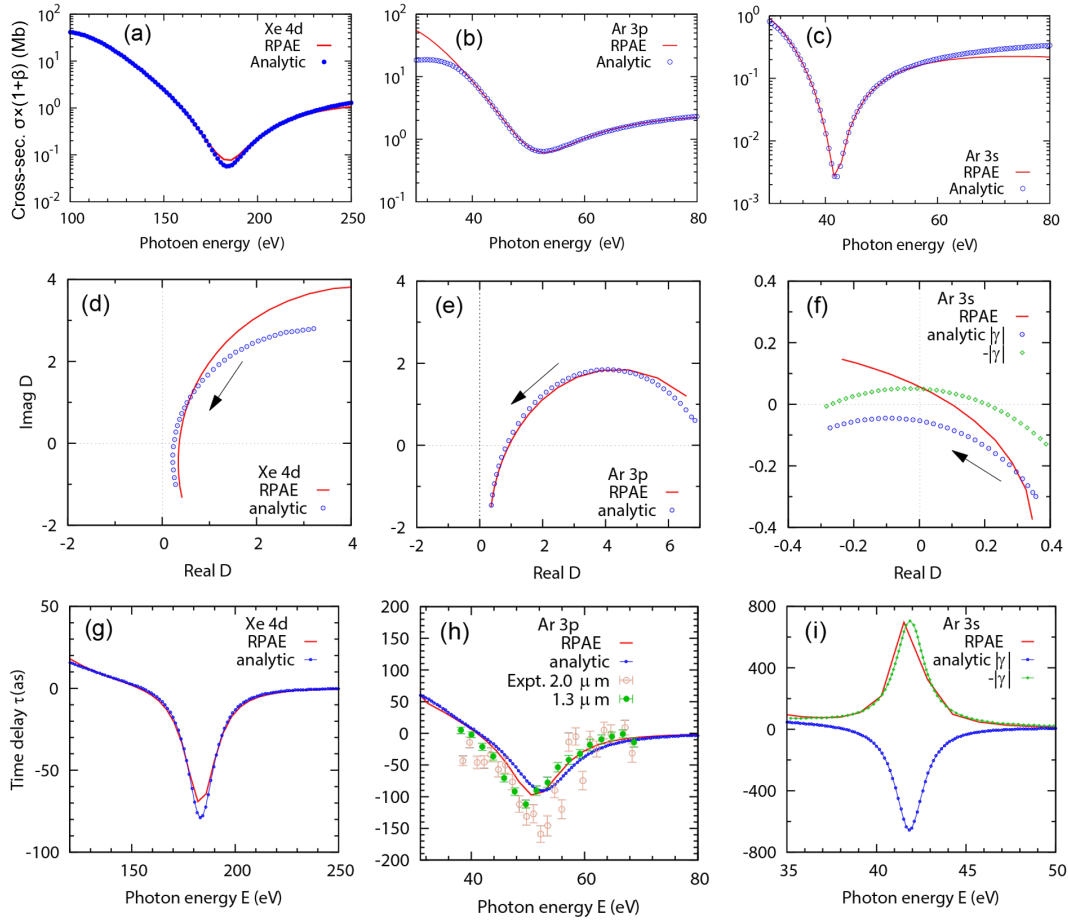


**Figure 5. Comparison of the cross-section-time-delay relation of various Cooper minima.** The photoionization cross sections in the Cooper minima of Xe 4d (a), Ar 3p (b), and Ar 3s (c) from the RPAE calculations (solid red) are fitted with the Fano lineshape (15) (blue dots). The photoionisation amplitudes of Xe 4d (d), Ar 3p (e), and Ar 3s (f) computed by RPAE (red) and reconstructed from the Fano profile using (19) (blue) are compared. The corresponding time delays from RPAE and by the analytical formula in (3) are shown in (g-i).

troverstial and suggests a need for additional investigations. Our approach shows that this seemingly large change in delays can be caused by a small shift of the transition amplitude in the complex plane.

We note that our method is not restricted to atomic one-photon processes, since similar resonances have been found in molecular systems [17,19,20,26] and in two-photon transitions [18,75,84,85]. Our result bridges two kinds of experiments in atomic and molecular physics and broadens the understanding of attosecond processes.

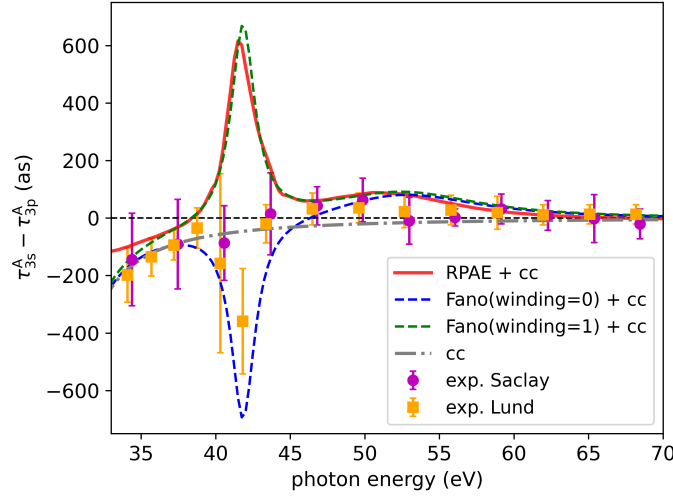


**Figure 6.** Experimental [24] and computed (RPAE, same as in figure 5) relative time delays between argon 3s and 3p, compared with the time delay retrieved from the Fano parameters using equations (18, 27). The contribution from the continuum-continuum (cc) transition due to the dressing IR field in the RABBIT measurement is addressed by adding an additional cc time delay given in [83].

## Appendix A. Formulation of the Lorentzian peak and the Fano peak

The Lorentzian line shape is given by

$$\sigma = \sigma_a \frac{1}{\epsilon^2 + 1} + \sigma_b = \sigma_b \frac{\epsilon^2 + 1 + \sigma_a/\sigma_b}{\epsilon^2 + 1}. \quad (\text{A.1})$$

Compared with (16), we have  $\mathfrak{S} = \sigma_b$ ,  $Q = 0$ , and  $\gamma^2 = 1 + \sigma_a/\sigma_b$ . For the Fano line shape,

$$\sigma = \sigma_a \frac{(\epsilon + q)^2}{\epsilon^2 + 1} + \sigma_b = (\sigma_a + \sigma_b) \frac{\epsilon^2 + \frac{2q\epsilon + q^2 + r}{r+1}}{\epsilon^2 + 1}. \quad (\text{A.2})$$

Compared with (16), we have  $\mathfrak{S} = \sigma_a + \sigma_b$ ,  $2Q = \frac{2q}{r+1}$  and  $Q^2 + \gamma^2 = \frac{q^2 + r}{r+1}$ , which leads to the expressions in the main text. From (16) we have

$$\frac{1}{\sigma} \frac{\partial \sigma}{\partial \epsilon} = \frac{2(\epsilon + Q)(\epsilon^2 + 1) - ((\epsilon + Q)^2 + \gamma^2) \cdot 2\epsilon}{((\epsilon + Q)^2 + \gamma^2)(\epsilon^2 + 1)} = \frac{2(\epsilon + Q)}{(\epsilon + Q)^2 + \gamma^2} - \frac{2\epsilon}{\epsilon^2 + 1} \quad (\text{A.3})$$

which yields expression (17).

## Appendix B. Phase-jump calculation

For  $\mathfrak{D}(\epsilon)$  in equation (19), we have

$$\text{Re}\{\mathfrak{D}(\epsilon)\}/\sqrt{\mathfrak{S}} = \frac{\epsilon^2 + Q\epsilon + \gamma}{\epsilon^2 + 1} \quad (\text{B.1})$$

$$\text{Im}\{\mathfrak{D}(\epsilon)\}/\sqrt{\mathfrak{S}} = \frac{(\gamma - 1)\epsilon - Q}{\epsilon^2 + 1}. \quad (\text{B.2})$$

It can be verified that

$$\left(\frac{\operatorname{Re}\{\mathfrak{D}(\epsilon)\}}{\sqrt{\mathfrak{E}}} - \frac{\gamma+1}{2}\right)^2 + \left(\frac{\operatorname{Im}\{\mathfrak{D}(\epsilon)\}}{\sqrt{\mathfrak{E}}} + \frac{Q}{2}\right)^2 = \frac{1}{4}((\gamma-1)^2 + Q^2). \quad (\text{B.3})$$

Hence, the trajectory of  $\mathfrak{D}(\epsilon)$  is a circle with the radius of  $\frac{\sqrt{\mathfrak{E}}}{2}\sqrt{(\gamma-1)^2 + Q^2}$  centred at  $\left(\sqrt{\mathfrak{E}}\frac{\gamma+1}{2}, -\sqrt{\mathfrak{E}}\frac{Q}{2}\right)$ . Since the origin is  $\frac{\sqrt{\mathfrak{E}}}{2}\sqrt{(\gamma+1)^2 + Q^2}$  away from the centre of the circle, the tangent segment from the origin is  $\sqrt{\mathfrak{E}}\sqrt{\gamma}$ , and the angle between the two tangents yields

$$|\Delta\phi|_{\max} = \max(\phi(\epsilon)) - \min(\phi(\epsilon)) = 2\cos^{-1}\left(\frac{2\sqrt{\gamma}}{\sqrt{(\gamma+1)^2 + Q^2}}\right). \quad (\text{B.4})$$

At  $\epsilon \rightarrow -\infty$ , the starting point of the trajectory approaches  $(\sqrt{\mathfrak{E}}, 0)$ , which is left to the centre when  $\gamma > 1$  while right to the centre when  $\gamma < 1$ . Since the trajectory evolves counter-clockwise, the phase between the two tangents increases when  $\gamma > 0$  and decreases when  $\gamma < 0$ . Therefore, the phase jump for  $\gamma \neq 1$  can be expressed as

$$\Delta\phi_{\max} = 2\operatorname{sgn}(\gamma-1)\cos^{-1}\left(\frac{2\sqrt{\gamma}}{\sqrt{(\gamma+1)^2 + Q^2}}\right). \quad (\text{B.5})$$

For  $\gamma = 1$ , it corresponds to a symmetric phase variation, where the maximal (minimal) phase is at  $\epsilon = 0$  while the minimal (maximal) phase is at  $\epsilon = \pm\infty$ , and

$$\begin{aligned} \phi^{\gamma=1}(0) - \phi^{\gamma=1}(\infty) &= -2\operatorname{sgn}(Q)\cos^{-1}\left(\frac{1}{\sqrt{1 + (Q/2)^2}}\right) \\ &= -2\tan^{-1}(Q/2). \end{aligned} \quad (\text{B.6})$$

In the special case of  $Q = 0$ , namely the Lorentzian peak, the expression can be simplified to

$$\Delta\phi_{\max}^{Q=0} = 4\tan^{-1}(\sqrt{\gamma}) - \pi \quad (\text{B.7})$$

which is positive when  $\gamma > 1$  (maximum in cross section) and is negative when  $\gamma < 1$  (minimum in cross section). It approaches  $+\pi$  and  $-\pi$  for  $\gamma \rightarrow +\infty$  ( $\sigma_b/\sigma_a \rightarrow -1$ ) and  $\gamma \rightarrow 0$  ( $\sigma_b/\sigma_a \rightarrow 0$ ), respectively.

## Appendix C. RPAE calculation

The RPAE calculations were performed using the ATOM program suite [86]. For argon, the correlations between the three optically allowed transitions  $3s \rightarrow Ep$  and  $3p \rightarrow Es/Ed$  were taken into account. For Xe  $4d$ , the five transitions  $5s \rightarrow Ep$ ,  $4p \rightarrow Es/Ed$  and  $4d \rightarrow Ep/Ed$  were included. The cross section in the polarization direction was evaluated from the total photoionization cross section and the angular anisotropy parameter as  $\sigma(1 + \beta)$ . The length gauge results were used for both  $\sigma$  and



$\beta$ . The time delay in the polarization direction was evaluated from the photoionization amplitude as in [28]. Summation over the magnetic projections in the ground state was reduced to  $m_i = 0$ .

## Appendix D. Fano parameters for cross sections near Cooper minima

The cross section of a Fano resonance can be conventionally expressed as [70, 71, 80]:

$$\sigma_F(\epsilon) = \sigma_0(\epsilon) \left( \rho^2 \frac{(q + \epsilon)^2}{1 + \epsilon^2} + 1 - \rho^2 \right) \quad (\text{D.1})$$

where  $\epsilon = (E - E_r)/(\Gamma/2)$ , and  $\rho^2$  is known as the correlation coefficient, and it is linked to equation (15) by letting  $\sigma_a = \rho^2 \sigma_0$ ,  $\sigma_b = (1 - \rho^2) \sigma_0$ ,  $r = \sigma_b/\sigma_a = 1/\rho^2 - 1$ , and approximating  $r$  as a constant across the CM. From the RPAE calculation, the Fano parameters are  $E_r = 105.46$  eV,  $\Gamma = 64.0282$  eV,  $\sigma_0 = 6.26653$  Mb,  $q = -2.45287$ ,  $\rho^2 = 0.990963$  for Xe  $4d$  CM,  $E_r = 29.2918$  eV,  $\Gamma = 18.468$  eV,  $\sigma_0 = 8.62031$  Mb,  $q = -2.67896$ ,  $\rho^2 = 0.934333$  for Ar  $3p$  CM, and  $E_r = 31.4118$  eV,  $\Gamma = 19.6322$  eV,  $\sigma_0 = 0.567772$  Mb,  $q = -1.06661$ ,  $\rho^2 = 0.995518$  for Ar  $3s$  CM, respectively, which correspond to the fitted curves in figure 5.

## Acknowledgements

J.-B.Ji acknowledges the funding from the ETH grant 41-20-2. M.H.'s work was funded by the European Union's Horizon 2020 research and innovation programme under Marie Skłodowska-Curie agreement grant No. 801459, FP-RESOMUS. J.-B.Ji thanks S. Luo (Jilin University), J. O. Richardson (ETH Zürich) and R. R. Lucchese (Lawrence Berkeley National Laboratory) for discussions.

## Author contributions statement

J.-B.J. derived the formulae with support of A.S.K., M.H., and K.U. A.S.K. performed the RPAE calculation and the fitting. J.-B.J., K.U., and H.J.W. conceived the study. M.H., K.U., and H.J.W. supervised its realization. All authors discussed the results and wrote the paper.

## Competing interests statement

All co-authors have seen and agree with the contents of the manuscript and there is no financial interest to report.

## References

- [1] Becker U and Shirley D A 1996 *VUV and Soft X-ray Photoionization* (Plenum Press)

- [2] Schmidt V 1997 *Electron Spectrometry of Atoms using Synchrotron Radiation* Cambridge Monographs on Atomic, Molecular and Chemical Physics (Cambridge University Press)
- [3] Corkum P B and Krausz F 2007 *Nature Physics* **3** 381–387
- [4] Krausz F and Ivanov M 2009 *Rev. Mod. Phys.* **81**(1) 163–234 URL <https://link.aps.org/doi/10.1103/RevModPhys.81.163>
- [5] Itatani J, Quéré F, Yudin G L, Ivanov M Y, Krausz F and Corkum P B 2002 *Phys. Rev. Lett.* **88** 173903
- [6] Kienberger R, Goulielmakis E, Uiberacker M, Baltuska A, Yakovlev V, Bammer F, Scrinzi A, Westerwalbesloh T, Kleineberg U, Heinzmann U, Drescher M and Krausz F 2003 *Nature* **427** 817–821
- [7] Véliard V, Taïeb R and Maquet A 1996 *Physical Review. A* **54**(1) 721–728 URL <https://link.aps.org/doi/10.1103/PhysRevA.54.721>
- [8] Paul P M, Toma E S, Breger P, Mullot G, Augé F, Balcou P, Muller H G and Agostini P 2001 *Science* **292** 1689
- [9] Schultze M, Fiess M, Karpowicz N, Gagnon J, Korbman M, Hofstetter M, Neppl S, Cavalieri A L, Komminos Y, Mercouris T, Nicolaides C A, Pazourek R, Nägele S, Feist J, Burgdörfer J, Azzeer A M, Ernstorfer R, Kienberger R, Kleineberg U, Goulielmakis E, Krausz F and Yakovlev V S 2010 *Science* **328** 1658–1662 URL <http://www.sciencemag.org/cgi/content/abstract/328/5986/1658>
- [10] Klünder K, Dahlström J M, Gisselbrecht M, Fordell T, Swoboda M, Guénot D, Johnsson P, Caillat J, Mauritsson J, Maquet A, Taïeb and L’Huillier A 2011 *Physical Review Letters* **106**(14) 143002 URL <http://link.aps.org/doi/10.1103/PhysRevLett.106.143002>
- [11] Eisenbud L 1948 *The formal properties of nuclear collisions* (Princeton University)
- [12] Wigner E P 1955 *Physical Review* **98** 145
- [13] Smith F T 1960 *Physical Review* **118** 349
- [14] Kotur M, Guenot D, Jiménez-Galán Á, Kroon D, Larsen E W, Louisy M, Bengtsson S, Miranda M, Mauritsson J, Arnold C *et al.* 2016 *Nature Communications* **7** 1–6
- [15] Gruson V, Barreau L, Jiménez-Galan Á, Risoud F, Caillat J, Maquet A, Carré B, Lepetit F, Hergott J F, Ruchon T, Argenti L, Taïeb R, Martín F and Salières P 2016 *Science* **354** 734–738 ISSN 0036-8075 URL <http://science.sciencemag.org/content/354/6313/734>
- [16] Zhong S, Vinbladh J, Busto D, Squibb R J, Isinger M, Neoričić L, Laurell H, Weissenbilder R, Arnold C L, Feifel R *et al.* 2020 *Nature Communications* **11** 1–6
- [17] Huppert M, Jordan I, Baykusheva D, Von Conta A and Wörner H J 2016 *Physical Review Letters* **117** 093001
- [18] Baykusheva D and Wörner H J 2017 *The Journal of Chemical Physics* **146** 124306 ISSN 0021-9606 URL <http://dx.doi.org/10.1063/1.4977933>
- [19] Heck S, Baykusheva D, Han M, Ji J B, Perry C, Gong X and Wörner H J 2021 *Science Advances* **7** eabj8121
- [20] Nandi S, Plésiat E, Zhong S, Palacios A, Busto D, Isinger M, Neoričić L, Arnold C, Squibb R, Feifel R *et al.* 2020 *Science Advances* **6** eaba7762
- [21] Heck S, Han M, Jelovina D, Ji J B, Perry C, Gong X, Lucchese R, Ueda K and Wörner H J 2022 *Physical Review Letters* **129** 133002
- [22] Hammerland D, Berglitsch T, Zhang P, Luu T T, Ueda K, Lucchese R R and Wörner H J 2024 *Science Advances* **10** eadl3810
- [23] Schoun S, Chirla R, Wheeler J, Roedig C, Agostini P, DiMauro L, Schafer K and Gaarde M 2014 *Physical Review Letters* **112** 153001
- [24] Alexandridi C, Platzer D, Barreau L, Busto D, Zhong S, Turconi M, Neoričić L, Laurell H, Arnold C, Borot A *et al.* 2021 *Physical Review Research* **3** L012012
- [25] Kheifets A S and Catsamas S 2023 *Physical Review A* **107** L021102
- [26] Holzmeier F, Joseph J, Houver J C, Lebech M, Doweck D and Lucchese R R 2021 *Nature Communications* **12** 1–9

- [27] Guenot D, Klünder K, Arnold C, Kroon D, Dahlström J M, Miranda M, Fordell T, Gisselbrecht M, Johnsson P, Mauritsson J *et al.* 2012 *Physical Review A* **85** 053424
- [28] Kheifets A 2013 *Physical Review A* **87** 063404
- [29] Magrakvelidze M, Madjet M E A, Dixit G, Ivanov M i and Chakraborty H S 2015 *Phys. Rev. A* **91**(6) 063415 URL <https://link.aps.org/doi/10.1103/PhysRevA.91.063415>
- [30] Dixit G, Chakraborty H S and Madjet M E A 2013 *Physical Review Letters* **111** 203003
- [31] Pi L W and Landsman A S 2018 *Applied Sciences* **8** 322
- [32] Hilborn R C 1982 *American Journal of Physics* **50** 982–986
- [33] Natalense A P P and Lucchese R R 1999 *J. Chem. Phys.* **111** 5344–5348 URL <http://link.aip.org/link/?JCP/111/5344/1>
- [34] Pazourek R, Nagele S and Burgdörfer J 2015 *Reviews of Modern Physics* **87** 765
- [35] Wigner E P and Eisenbud L 1947 *Physical Review* **72** 29
- [36] Kelkar N and Nowakowski M 2008 *Physical Review A* **78** 012709
- [37] Schützer W and Tiomno J 1951 *Physical Review* **83** 249
- [38] Van Kampen N 1953 *Physical Review* **91** 1267
- [39] Gell-Mann M, Goldberger M and Thirring W E 1954 *Physical Review* **95** 1612
- [40] Goldberger M L 1955 *Physical Review* **97** 508
- [41] Karplus R and Ruderman M A 1955 *Physical Review* **98** 771
- [42] Khuri N N 1957 *Physical Review* **107** 1148
- [43] Meiman M 1964 *Sov. Phys. JETP* **47** 188
- [44] Taylor J R 1972 *Scattering theory: the quantum theory of nonrelativistic collisions* (John Wiley & Sons, Inc.)
- [45] Rescigno T N and Reinhardt W P 1973 *Physical Review A* **8** 2828
- [46] Reinhardt W P 1982 *Annual Review of Physical Chemistry* **33** 223–255
- [47] Moiseyev N 1998 *Physics Reports* **302** 212–293
- [48] Branson D 1964 *Physical Review* **135** B1255
- [49] Eden R and Landshoff P 1965 *Annals of Physics* **31** 370–390
- [50] Peres A 1966 *Annals of Physics* **37** 179–208
- [51] Kramers H A 1924 *Nature* **113** 673–674
- [52] de L Kronig R 1926 *J. Opt. Soc. Am.* **12** 547–557 URL <https://opg.optica.org/abstract.cfm?URI=josa-12-6-547>
- [53] Kramers H A 1927 La diffusion de la lumière par les atomes *Atti Cong. Intern. Fisica (Transactions of Volta Centenary Congress) Como* vol 2 pp 545–557
- [54] Abbamonte P, Finkelstein K, Collins M and Gruner S 2004 *Physical Review Letters* **92** 237401
- [55] Ott C, Kaldun A, Raith P, Meyer K, Laux M, Evers J, Keitel C H, Greene C H and Pfeifer T 2013 *Science* **340** 716–720
- [56] Stooß V, Cavaletto S M, Donsa S, Blättermann A, Birk P, Keitel C H, Březinová I, Burgdörfer J, Ott C and Pfeifer T 2018 *Physical Review Letters* **121** 173005
- [57] Lee Y W 1932 *Journal of Mathematics and Physics* **11** 83–113
- [58] Bode H W *et al.* 1945 *Network analysis and feedback amplifier design* (van Nostrand)
- [59] Raymond F H 1951 *Annales Des Télécommunications* **6** 262–272
- [60] Hoenders B 1975 *Journal of Mathematical Physics* **16** 1719–1725
- [61] Burge R, Fiddy M, Greenaway A and Ross G 1976 *Proceedings of the Royal Society of London. A. Mathematical and Physical Sciences* **350** 191–212
- [62] Mecozzi A 2009 *Optics Communications* **282** 4183–4187
- [63] Mecozzi A 2016 *arXiv preprint arXiv:1606.04861* URL <https://arxiv.org/abs/1606.04861>
- [64] Shilov G E 1996 *Convergence of Improper Integrals* (New York: Dover Publications) pp 438–443  
Dover books on mathematics revised english ed ISBN 0486689220
- [65] Zorich V A 2016 *Integrals Depending on a Parameter* (Berlin, Heidelberg: Springer Berlin Heidelberg) pp 405–492 ISBN 978-3-662-48993-2 URL [https://doi.org/10.1007/978-3-662-48993-2\\_9](https://doi.org/10.1007/978-3-662-48993-2_9)

- [66] Pollak E and Miller W H 1984 *Physical Review Letters* **53** 115
- [67] Yamada N 2004 *Physical Review Letters* **93** 170401
- [68] Breit G and Wigner E 1936 *Physical Review* **49** 519
- [69] Friedrich H 2017 *Theoretical atomic physics* (Springer International Publishing)
- [70] Fano U 1961 *Physical Review* **124** 1866
- [71] Fano U and Cooper J 1965 *Physical Review* **137** A1364
- [72] Feshbach H 1962 *Annals of Physics* **19** 287–313
- [73] Ma Z R, Huang X C, Li T J, Wang H C, Liu G C, Wang Z S, Li B, Li W B, Zhu L F *et al.* 2022 *Physical Review Letters* **129** 213602
- [74] Goldberger M L and Watson K M 1962 *Physical Review* **127** 2284
- [75] Argenti L, Jiménez-Galán Á, Caillat J, Taïeb R, Maquet A and Martín F 2017 *Physical Review A* **95** 043426
- [76] Deshmukh P, Mandal A, Saha S, Kheifets A, Dolmatov V and Manson S 2014 *Physical Review A* **89** 053424
- [77] Bray A W, Naseem F and Kheifets A S 2018 *Physical Review A* **98** 043427
- [78] Cooper J W 1962 *Phys. Rev.* **128** 681
- [79] Wörner H J, Niikura H, Bertrand J B, Corkum P B and Villeneuve D M 2009 *Physical Review Letters* **102** 103901 URL <http://link.aps.org/abstract/PRL/v102/e103901>
- [80] Kossmann H, Krassig B and Schmidt V 1988 *Journal of Physics B: Atomic, Molecular and Optical Physics* **21** 1489
- [81] Shiner A D, Schmidt B, Trallero-Herrero C, Wörner H J, Patchkovskii S, Corkum P B, Kieffer J C, Légaré F and Villeneuve D M 2011 *Nat. Phys.* **7** 464–467 URL <http://link.aps.org/abstract/PRL/v103/e073902>
- [82] Kheifets A S 2023 *Journal of Physics B: Atomic, Molecular and Optical Physics* **56** 022001
- [83] Dahlström J M and Lindroth E 2014 *Journal of Physics B: Atomic, Molecular and Optical Physics* **47** 124012
- [84] Jiménez-Galán Á, Argenti L and Martín F 2014 *Physical Review Letters* **113** 263001
- [85] Jiménez-Galán Á, Martín F and Argenti L 2016 *Physical Review A* **93** 023429
- [86] Amusia M I and Chernysheva L V 1997 *Computation of atomic processes : A handbook for the ATOM programs* (Bristol, UK: Institute of Physics Pub.)